High-Speed 9.6-μm Long-Wave Infrared Free-Space Transmission With a Directly-Modulated QCL and a Fully-Passive QCD

Mahdieh Joharifar, Hamza Dely, Xiaodan Pang, *Senior Member, IEEE*, Richard Schatz, Djamal Gacemi, Toms Salgals, Aleksejs Udalcovs, *Senior Member, IEEE*, Yan-Ting Sun, Yuchuan Fan, Lu Zhang, Etienne Rodriguez, Sandis Spolitis, Vjaceslavs Bobrovs, Xianbin Yu, *Senior Member, IEEE*, Sebastian Lourdudoss, *Senior Member, IEEE*, Sergei Popov, Angela Vasanelli, Oskars Ozolins, *Senior Member, IEEE*, and Carlo Sirtori

(Post-Deadline Paper)

***Abstract*—Free-space optics (FSO) in the mid-infrared (mid-IR) contains rich spectral resources for future ultrahigh-speed wireless communications yet is currently under-exploited. Two atmospheric transmission windows at the mid-IR, namely, the mid-wave IR (MWIR, 3–5 μm) and the long-wave IR (LWIR, 8–12 μm), show great potential in supporting free-space communications for both terrestrial and space application scenarios. Particularly, the LWIR signal with a longer wavelength has high intrinsic robustness against aerosols' scattering and turbulence-induced scintillation and beam broadening effects, which are the main concerns hindering the wide deployment of practical FSO systems. In this context, high-bandwidth semiconductor-based mid-IR FSO transceivers will be desirable to meet the requirements of low energy consumption and small footprints for large-volume development and deployment. Quantum cascade devices, including quantum cascade lasers (QCLs) and quantum cascade detectors (QCDs), appear promising candidates to fulfill this role. In this work, we report a high-speed LWIR FSO transmission demonstration with a 9.6-μm directly-modulated (DM)-QCL and a fully passive QCD without any active cooling or bias voltage. Up to 8 Gb/s, 10 Gb/s, and 11 Gb/s signal transmissions are achieved when operating the DM-QCL at 10 °C, 5 °C, and 0 °C, respectively. These results indicate a significant step towards an envisioned fully-connected mid-IR FSO solution empowered by the quantum cascade semiconductor devices.**

***Index Terms*—Free-space optics, long-wave infrared, quantum cascade detector, quantum cascade laser.**

Manuscript received 14 June 2022; revised 31 August 2022; accepted 12 September 2022. Date of publication 15 September 2022; date of current version 16 February 2023. This work was supported in part by the EU H2020 cFLOW Project under Grant 828893, in part by the ENS-THALES Chair, in part by the Swedish Research Council (VR) under Grants 2019-05197 and 2016-04510, in part by the COST Action CA19111 NEWFOCUS, in part by the ERDF-funded CARAT under Grant 1.1.1.2/VIAA/4/20/660, and in part by the RTU Science Support Fund. *(Mahdieh Joharifar and Hamza Dely contributed equally to this work.) (Corresponding authors: Xiaodan Pang; Carlo Sirtori.)*

Mahdieh Joharifar, Richard Schatz, Yan-Ting Sun, Yuchuan Fan, Sebastian Lourdudoss, and Sergei Popov are with the Department of Applied Physics, KTH Royal Institute of Technology, 106 91 Stockholm, Sweden (e-mail: mahdieh@kth.se; rschatz@kth.se; yasun@kth.se; yuchuanf@kth.se; slo@kth.se; sergeip@kth.se).

Hamza Dely, Djamal Gacemi, Etienne Rodriguez, Angela Vasanelli, and Carlo Sirtori are with the Laboratoire de Physique de l'École Normale Supérieures, ENS, Université PSL, CNRS, Sorbonne Université, Université de Paris, 75005 Paris, France (e-mail: hamza.dely@ens.fr; djamal.gacemi@phys.ens.fr; etienne.rodriguez@phys.ens.fr; angela.vasanelli@phys.ens.fr; carlo.sirtori@phys.ens.fr).

Xiaodan Pang is with the Department of Applied Physics, KTH Royal Institute of Technology, 106 91 Stockholm, Sweden, with the RISE Research Institutes of Sweden, 164 40 Kista, Sweden, and also with the Institute of Telecommunications, Riga Technical University, 1048 Riga, Latvia (e-mail: xiaodan@kth.se).

Toms Salgals and Sandis Spolitis are with the Institute of Telecommunications, Riga Technical University, 1048 Riga, Latvia, and also with the Communication Technologies Research Center, Riga Technical University, 1048 Riga, Latvia (e-mail: toms.salgals@rtu.lv; sandis.spolitis@rtu.lv).

Aleksejs Udalcovs is with the RISE Research Institutes of Sweden, 164 40 Kista, Sweden (e-mail: aleksejs.udalcovs@gmail.com).

Lu Zhang and Xianbin Yu are with the College of Information Science and Electronic Engineering, Zhejiang University, Hangzhou 310027, China, and also with Zhejiang Lab, Hangzhou 310000, China (e-mail: zhanglu1993@zju.edu.cn; xyu@zju.edu.cn).

Vjaceslavs Bobrovs is with the Institute of Telecommunications, Riga Technical University, 1048 Riga, Latvia (e-mail: vjaceslavs.bobrovs@rtu.lv).

Oskars Ozolins is with the Department of Applied Physics, KTH Royal Institute of Technology, 106 91 Stockholm, Sweden, with the RISE Research Institutes of Sweden, 164 40 Kista, Sweden, and also with the Institute of Telecommunications, Riga Technical University, 1048 Riga, Latvia (e-mail: oskars.ozolins@ri.se).

Color versions of one or more figures in this article are available at https://doi.org/10.1109/JLT.2022.3207010.

Digital Object Identifier 10.1109/JLT.2022.3207010

I. Introduction

FREE-SPACE optics (FSO) has recently emerged as a potential candidate to complement the radio technologies for both terrestrial and space communications, including ground-to-satellite and inter-satellite communications. Extrapolating the applications and requirements of the fifth-generation (5G) mobile networks currently being deployed, one may anticipate at least two orders of magnitude higher data rate demand for the next-generation wireless communication technologies, i.e., the 6G [1]. Subsequently, an all-spectra communication paradigm facilitating cooperative free-space communications with both optics and radio has been proposed to offer the required ultra-broad spectral resources [2]. Among all the options spanning from the microwave to the ultraviolet (UV), the spectral region across the terahertz (THz) band, i.e., from 0.3 THz to tens of THz, where the mid- and far-infrared (IR) optics and

sub-millimeter-wave (MMW) radio overlap, has a relatively lower technology readiness level compared with other spectral windows [3]. Particularly, the two atmospheric transmission windows at the mid-wave IR (MWIR, 3–5 μm, 60–100 THz) and the long-wave IR (LWIR, 8–12 μm, 25–37 THz) in the mid-infrared (MIR) region (wavelength range of 3–50 μm) contain a rich potential for FSO technologies and communication purposes, yet to be exploited. Compared with the MMW and sub-THz bands being heavily studied and discussed for 6G wireless communications, the MWIR and LWIR have almost two orders of magnitude lower atmospheric propagation attenuation with a tenfold broader fully unlicensed bandwidth [4]. On the other hand, compared with the 1.5-μm telecom band in the short-wave IR (SWIR, 1–2.5 μm), where most commercial FSO communications are developed, the MWIR and LWIR have much higher resilience against adverse weather, e.g., much lower sensitivity to particle scattering atmospheric turbulence effects [5]. Moreover, the mid-IR region shows a lower risk for eye safety [6].

An often-adopted approach to carrying out mid-IR FSO system demonstrations is using wavelength conversions [7], [8], [9], [10], [11], [12]. This approach utilizes the well-developed telecom transceivers and converts the signal wavelength between 1.5 μm and mid-IR based on difference frequency generation (DFG) before and after the FSO link. Recent studies with such an approach have reported very high data rates. For example, single-channel transmissions of 10 Gb/s in-phase and quadrature (IQ) modulated signals have been demonstrated [10], [11]. Moreover, with wavelength- and mode-division multiplexing techniques, MIR FSO transmissions with a total data rate of 300 Gb/s have been achieved at 3.4 μm [12]. However, the high-power consumption associated with the nonlinear wavelength conversion in such methods leads to energy deficiency and hardware complexity, obstructing practical development. A more attractive choice in the long-term would be direct-emission semiconductor lasers and photodetectors.

Quantum cascade devices, including quantum cascade lasers (QCLs) [13] and quantum cascade detectors (QCDs) [14], are based on inter-subband transitions to cover a wide spectral range from the MIR to THz. They appear as promising candidates due to their breakthroughs in a broad bandwidth, high-temperature operation, and low energy consumption [15], [16], [17], [18]. Particularly, directly modulated (DM)-QCLs have ultra-short carrier relaxation lifetime, leading to a high intrinsic modulation bandwidth and making the laser response over-damped, thus repressing the resonance frequency [19], [20]. In recent years, high bandwidth modulation of QCLs operated at room temperature has rekindled a new wave of interest in studying QCL-based FSO communication systems [21]. There have been several reports of free-space transmission demonstrations using DM-QCLs at room temperature [22], [23], [24], [25]. Among these works, the highest reported bitrate of 6 Gb/s is achieved in the MWIR region of 4.65 μm with a thermoelectric-cooled Mercury-Cadmium-Telluride (HgCdTe) photovoltaic (PV) detector operating at 200 K to assure the low-noise characteristics [25]. The LWIR range, which has a smaller energy bandgap than the MWIR, imposes more stringent requirements for the power and noise characteristics of the device [26], [27]. Before this work, the highest reported bitrate for LWIR FSO at room temperature with DM-QCL, to the best of our knowledge, was up to 2 Gb/s with a bit error rate (BER) below the 2×10^{-2} soft-decision (SD) forward error correction (FEC) limit [28]. Lately, a 9-μm FSO data transmission based on an external free-space Stark modulator and an unbiased QCD without any active cooling was reported and up to 10 Gb/s non-return-to-zero on-off keying (NRZ-OOK) signals at room temperature was demonstrated [29], [30]. However, the external modulator-based FSO systems require extra LWIR optics and a more delicate beam alignment to collimate and gain the optimum power. These extra efforts are imperative to increase the modulation depth, thus achieving the required signal-to-noise ratio (SNR) at the detector. Therefore, a more efficient and straightforward candidate is DM-QCL which can accelerate commercial LWIR FSO solutions in the short term, whereas future maturity of external-modulation technologies may bring improved modulation bandwidth and quality in the long term.

In this paper, we extend our recent report on high-speed LWIR DM-QCL-based FSO demonstration [31] with more detailed system characterizations and transmission performance evaluations. For different temperatures from 10 °C down to 0 °C, we experimentally compare two modulation formats, i.e., NRZ-OOK and 4-level pulse-amplitude modulation (PAM4), and benchmark their respective maximum data rate against the 6.25% overhead (OH) hard-decision (HD) FEC limit [32]. We show that up to 8 Gb/s, 10 Gb/s, and 11 Gb/s PAM4 transmissions can be achieved at operating temperatures of 10 °C, 5 °C, and 0 °C, respectively, with the 9.6-μm DM-QCL and an uncooled and unbiased passive QCD.

The rest of this paper is organized as follows: in Section II, we present the key characteristics of the DM-QCL and the QCD and describe the experimental configurations of the transmission system. Section III shows the measurement results of the LWIR transmissions at three different temperature values. Finally, we give our conclusions in Section IV.

II. Experimental Configuration

A. Characteristics of the Quantum Cascade Components

The DM-QCL used in our experiment is a 3-mm distributed-feedback (DFB) ridge laser fabricated epi-down. In this way, the laser chip can be operated at room temperature with the help of a Peltier thermoelectric controller (TEC). The laser chip was soldered on a sub-mount and then wire bonded to a high-frequency coplanar waveguide. Fig. 1(a) shows the picture of the QCL mount and the zoomed view of the DFB-QCL chip. The output of the DM-QCL is a continuous wave centered at a wavelength of 9.6 μm with a few tens of milliwatts of output power. The device has a cut-off modulation frequency of around 3 GHz, beyond which the frequency response drops drastically. In our transmission system experiment, we use a Peltier TEC to stabilize the DM-QCL operation temperature at three different points, i.e., 10 °C, 5 °C, and 0 °C. Fig. 1(b) shows the characterized L-I-V curve of the laser at the selected operating temperature values. One can observe that the DM QCL starts lasing around 560 mA injection current at all investigated temperatures and saturates at around 675 mA. It is noted that due

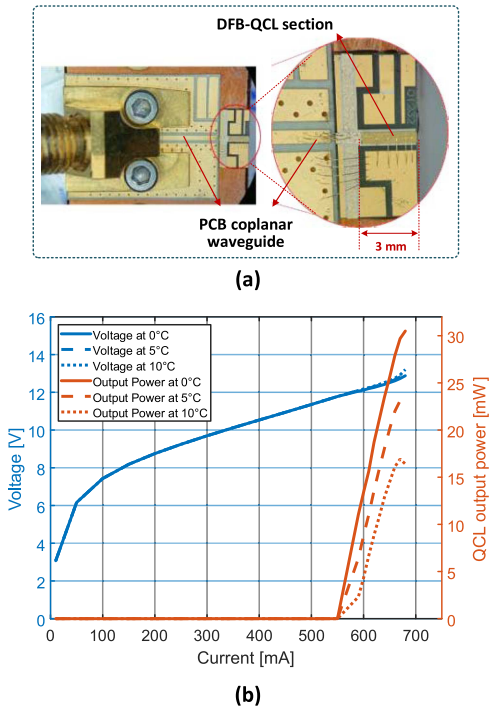

Fig. 1. (a) The PCB hosting the 9.6-μm DFB-QCL chip that is wire bonded to a coplanar waveguide delivering the bias and RF modulation signals. (b) The measured L-I-V curves of the QCL at operation temperature of 0 °C, 5 °C and 10 °C, respectively.

to the large measurement steps around the threshold current, the slight differences between the thresholds at different temperatures couldn't be distinguished. For the same reason, the L-I curve for the case of 10 °C also appears piecewise linear near the threshold, which is a measurement artifact. Lower operation temperature enables a higher output power, and the maximum achieved output power at 10 °C, 5 °C, and 0 °C are 16.4 mW, 23.4 mW, and 30.5 mW, respectively.

The LWIR FSO receiver for this experiment is a fully passive GaAs/AlGaAs QCD without any bias or cooling, operating in a room-temperature environment (no air conditioning, temperature drifting between 25 °C and 30 °C). Fig. 2 shows the picture and the characteristics of the employed QCD. The detector was fabricated into a 55×55 μm^2 square mesa structure where the top contact is realized with an air bridge. Such a mesa structure is used to operate at high frequencies, compared with traditional mesa structures with larger sizes and long wire bonds usually used for static / low-frequency measurements. The air bridge is continued by a coplanar waveguide on the GaAs substrate, which is then connected through short wire bonds to a printed circuit board (PCB) coplanar waveguide equipped with a 2.92-mm connector. The QCD is based on a diagonal transition with a 45 ° polished facet that satisfies the polarization requirements for optical transitions [33]. This unipolar detector conducts in the photovoltaic regime; yet has s a very wideband frequency range with a first-order roll-off. This behavior is due to the fast energy relaxation of the electrons as the only charge carriers. Also, the asymmetry of the cascade region that acts as a pseudo-electric

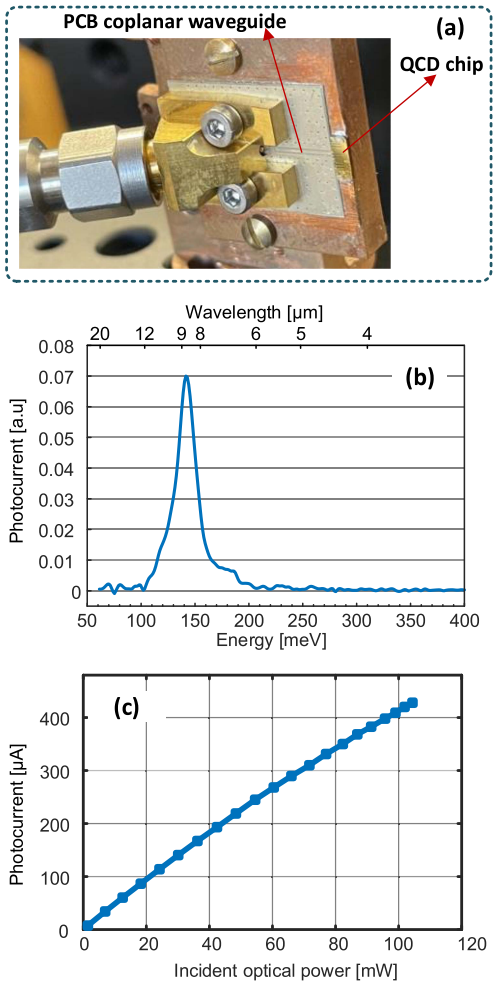

Fig. 2. (a) The picture of the hosting PCB for the QCD chip. (b) The measured photocurrent spectrum of the QCD at room temperature as a function of both the photon energy and the corresponding wavelength. (c) The measured photocurrent of the uncooled QCD as a function of incident CW optical power.

lead to a photocurrent. The cascade region is designed in such a way that the electron relaxation lifetime from one period to the adjacent one is estimated to be shorter than 10 ps. Therefore, the intrinsic bandwidth, in theory, can be in the order of 100 GHz [34]. In practice, the bandwidth is often limited by electrical parasitic capacitance in the mesa structure, packaging, and driving circuit. For this particular device, the cut-off frequency is around 6 GHz due to both the RF packaging and the impedance mismatch. Per the previous measurement, the detector has an almost flat frequency response up to its cut-off frequency [29]. Fig. 2(a) shows a picture of the QCD mount where the detector chip is wire-bonded to the coplanar waveguide. Fig. 2(b) shows the photocurrent characterization of the QCD at room temperature. The peak responsivity is measured at 141.6 meV photon energy, corresponding to 8.75 μm of wavelength. While at 9.6 μm, the detector responsivity performance drops to approximately 45%. Therefore, we can expect improved efficiency with a lightly shorter laser wavelength approaching the peak. As shown in Fig. 2(c), the photocurrent of the QCD has a linear relation with

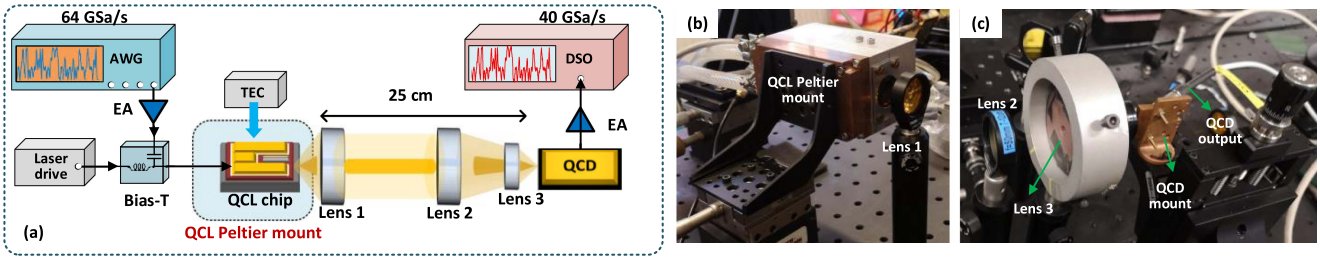

Fig. 3. (a) The experimental setup of the LWIR FSO transmission link. AWG: arbitrary waveform generator. EA: electrical amplifier. TEC: thermoelectric controller. DSO: digital storage oscilloscope. (b) The picture of the LWIR FSO transmitter with the QCL Peltier mount and the collimating lens. (c) The picture of the LWIR FSO receiver with cascaded beam focusing lenses and the QCD mount.

the injected optical power up to 50 mW with a responsivity of 4.5 mA/W at 9 μm at room temperature. In our transmission experiment, the highest optical power measured on the detector was 30.5 mW within the linear region.

B. Transmission Setup of the LWIR FSO System

Fig. 3(a) shows the experimental setup of the LWIR FSO transmission system. We use a 64 GSa/s arbitrary waveform generator (AWG) to convert the offline generated digital signals into the analog domain. Two modulation formats are employed for system performance evaluation, i.e., NRZ-OOK and PAM4. Their symbols are mapped from a random binary sequence of $>$1 million unrepeated bit-length generated using the Mersenne Twister with a shuffled seed number. Then, the sequence was filtered with a root-raised-cosine (RRC) pulse shaping filter with a roll-off factor of 0.15 after optimization. To compensate for the bandwidth limitation of the system, we apply a static pre-emphasis finite impulse response (FIR) filter at the transmitter digital signal processing (DSP). The AWG output signal is amplified with a 30 dB-gain electrical amplifier (EA) to a peak-to-peak voltage of $>$2.5 V_{pp}. The value of the driving signal varies between the modulation formats and different baud rates. The signal is combined with the bias current at an external bias-tee and delivered to the DM-QCL. Subsequently, at the DM-QCL output, we installed a ZnSe aspheric lens to collect and collimate the emitted laser beam. A picture of the transmitter configuration is shown in Fig. 3(b).

In this experiment, the FSO link distance was set to 25 cm to simplify the beam alignment and collimation. To achieve the maximum photocurrent value at the QCD, we placed an optical beam focusing element consisting of two cascaded lenses to focus the light on the detector to obtain the smallest spot size possible. Such an focusing configuration allowed us achieving a "best-effort" coupling efficiency into the detector, thus ensuring sufficient receiver SNR for the FSO transmissions. Fig. 3(c) shows the photos of the LWIR FSO receiver configuration. Before data transmission, we optimized the beam alignment using an optical chopper of 1 kHz and a lock-in amplifier while keeping the QCL unmodulated with continuous-wave output. The lock-in amplifier was connected to the QCD output, so that maximizing the detected signal at 1 kHz by tuning the optomechanics at both the transmitter and receiver indicates optimal alignment. After optimal alignment is achieved, the detected signal from the QCD output is amplified with a 30 dB-gain electrical low-noise amplifier (LNA) and collected with a 40 GSa/s real-time digital storage oscilloscope (DSO). Finally, the sampled digital signal is processed with a matched filter, timing recovery, and down-sampling process based on maximum variance, a symbol-spaced decision-feedback equalizer (DFE) with 55-feedforward taps, and 55-feedback taps, and the BER performance is evaluated after the symbol-to-bit demodulation.

III. Experimental Results

This section presents the system-level experimental results. In our experiment, we operate the QCL at three different temperature values, i.e., 10 °C, 5 °C, and 0 °C, and explore the maximum supported data rates, respectively.

A. Results at 10 °C Temperature

Fig. 4 shows the characterized end-to-end amplitude and phase response of the system at 10 °C temperature, including the AWG, QCL, QCD, DSO, and all the electrical components that play a part in between. It's worth noting that for all temperature cases, the frequency response measurements were performed at optimal QCL bias points, taking into account the trade-off between SNR and linearity. For 10 °C, the end-to-end 3-dB bandwidth is found to be around 400 MHz, and the 10-dB bandwidth is around 1.6 GHz. In addition, two static, narrow frequency dips are observed at 580 MHz and 950 MHz, induced by the external bias-tee and the impedance mismatch between the bias-tee and the QCL RF input. These frequency dips are equalized digitally with both pre- and post-equalizers. Fig. 4(b) shows the measured phase response, which stays smooth up to the 3-dB bandwidth and starts fluctuating at higher frequencies due to the influence of noise in the system, limiting the measurement stability and accuracy.

After the frequency response characterization at 10 °C, we evaluate the system transmission performance with the two modulation formats, namely, NRZ-OOK and PAM4. At this temperature, maximum bit rates for each modulation format are explored against the 6.25%-OH HD-FEC limit. Moreover, because there is no variable attenuator in the experimental setup, we would face a lack of accuracy in tuning the optomechanics. Therefore, we keep the link setup untouched after optimizing

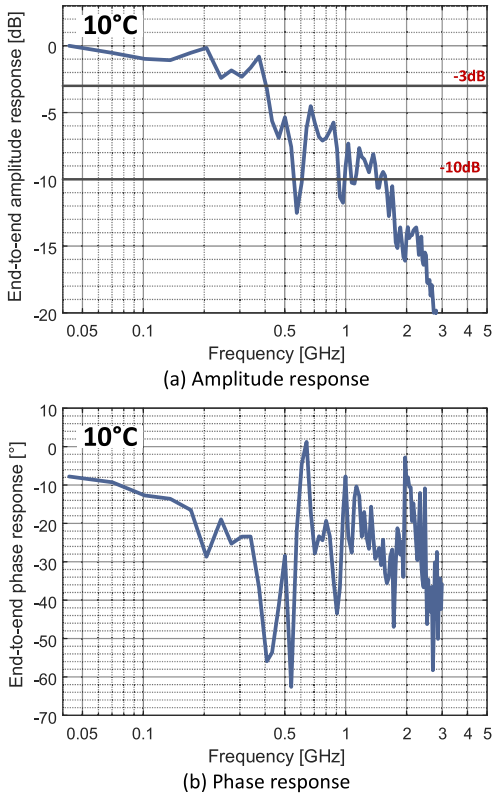

Fig. 4. The characterized (a) amplitude response and (b) phase response of the end-to-end system at 10 °C, including the responses of the DM-QCL, the QCD, and all the electrical and RF components and cables.

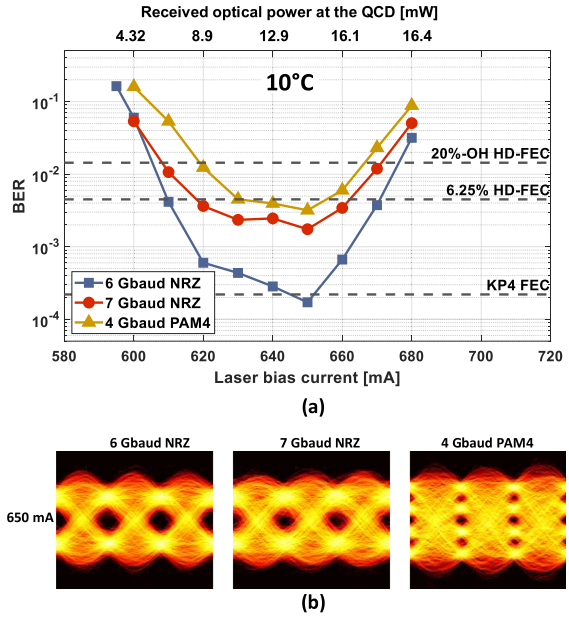

Fig. 5. (a) BER as a function of the laser bias current for NRZ-OOK signals at 6 Gbaud (6 Gb/s) and 7 Gbaud (7 Gb/s), and PAM4 signal at 4 Gbaud (8 Gb/s); (b) Selected eye diagrams for all three cases measured at the optimal laser bias value of 650 mA.

the beam alignment and evaluate the performance of the system transmission by sweeping the bias current of the DM-QCL, which subsequently changes the received optical power at the detector. Understandably, the bias current point of the laser is also correlated to the modulation linearity. Fig. 5(a) shows the BER performance as a function of the laser bias for three achievable signal configurations: NRZ-OOK at 6 Gbaud and 7 Gbaud, and PAM4 at 4 Gbaud, and the top axis is the corresponding received optical power at the detector. The optimum point of the bias current was detected at 650 mA, yielding 14.5 mW received optical power at the QCD to attain a sufficient signal SNR and the linearity simultaneously. Around the optimal bias point, BER performances below the 6.25%-OH HD-FEC limit are achievable for all three test cases. The 20%-OH HD-FEC and the KP4-FEC thresholds are shown in the figure only for reference. Further increasing the PAM4 baud rate to above 4 Gbaud would degrade the BER performance beyond the 6.25%-OH HD-FEC threshold, limited by the receiver SNR due to insufficient output power from the QCL at this temperature, as previously shown in Fig. 1(b). Selected eye diagrams after the post-equalizer for all the three cases at the optimal bias point are shown in Fig. 5(b). Clear eye openings with negligible nonlinear distortions are observed.

B. Results at 5 °C Temperature

We then decrease the QCL operating temperature to 5 °C and perform the same system-level evaluation as at 10 °C to explore the data rate limit. A higher data rate can be expected owing to higher output power from the QCL at a lower temperature. First, we characterize the system's end-to-end frequency response, and the measured results are shown in Fig. 6. One can observe only slight improvements in the 3-dB and the 10-dB bandwidth, whereas the same frequency dips remain at 580 MHz and 950 MHz due to unchanged hardware configuration. Due to the noise limit, similar phase fluctuation beyond the 3-dB bandwidth is again observed in Fig. 6(b). Fig. 7 shows the BER performance as a function of the QCL bias point. At this temperature, we manage to increase the baud rate of PAM4 to 5 Gbaud with BER performance below the 6.25%-OH HD-FEC limit. The optimal bias point throughout the current sweeping for PAM4 was found around 630 mA, corresponding to the received optical power of 15.9 mW. Fig. 7(b) shows the selected eye diagrams at different laser bias points for the 5 Gbaud PAM4 signal. It clearly indicates the compression of lower-amplitude levels at 600 mA for the PAM4 signal as it is too close to the QCL lasing threshold. On the other hand, increasing the bias current beyond the optimal point causes compression on the upper amplitude levels. It causes severe signal distortion at 680 mA, despite the high achievable SNR at this point. For the case of NRZ-OOK, as shown in Fig. 7(a), increasing from 7 Gbaud to 8 Gbaud fails to meet the targeted BER threshold of 4.5×10^{-3} due to the limited bandwidth and SNR. Another observation is that the optimal bias for NRZ-OOK is higher than PAM4 due to its higher tolerance to modulation nonlinearity.

C. Results at 0 °C Temperature

Finally, we characterize the system and evaluate the transmission performance at 0 °C. As shown in Fig. 8, similar frequency

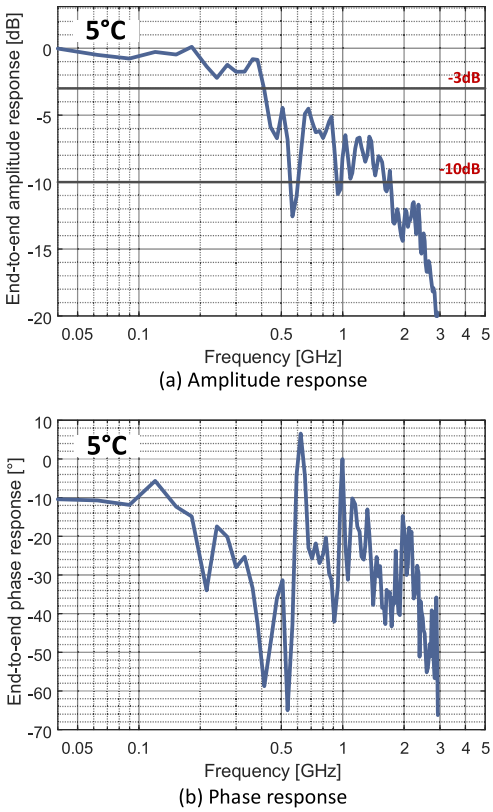

Fig. 6. The characterized (a) amplitude response and (b) phase response of the end-to-end system at 5 °C.

response in both amplitude and phase is obtained as operating at 5 °C. Fig. 9(a) shows the BER performance as a function of the laser bias for the two modulation formats. Due to the increased QCL output power, the highest achievable data rate can be further improved at this temperature. The optimal bias point was found between 630 mA and 640 mA, where both the 5.5 Gbaud PAM4 and the 8 Gbaud NRZ-OOK could achieve BER values that fulfill the 6.25%-OH HD-FEC requirement. Further increasing the PAM4 baud rate to 6 Gbaud fails to achieve BER performance below the targeted FEC threshold of 4.5×10^{-3} BER. Fig. 9(b) shows the equalized signal eye diagrams at several selected bias points for both 5.5 Gbaud PAM4 and 8 Gbaud NRZ-OOK. Again, the trade-off between the signal SNR and modulation linearity can be clearly observed by looking at the eye diagrams, particularly in the case of PAM4. A higher coding-gain FEC configuration, 20%-OH HD-FEC, may be used for further data rate enhancement, but it is considered an unfavored option due to its increased latency and complexity.

The transmission results achieved at all temperatures benchmarked against different FEC thresholds are summarized in Table I. Comparing the obtained results across all the tested temperature and bias cases, we conclude that the transmission performance is primarily determined by the trade-off between the SNR and the modulation linearity, as the impacts due to other factors such as wavelength shift and QCD thermal dissipation are identified negligible per our evaluation. Finally, it is worth noting that enhanced transmission speed and performance can be well

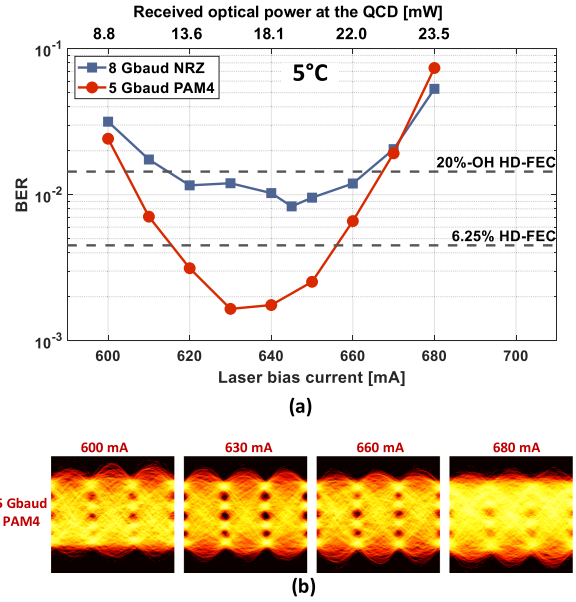

Fig. 7. (a) BER as a function of the laser bias current for NRZ-OOK signal at 8 Gbaud and PAM4 signal at 5 Gbaud (10 Gb/s); (b) Selected eye diagrams for 5 Gbaud PAM4 measured at different laser bias points.

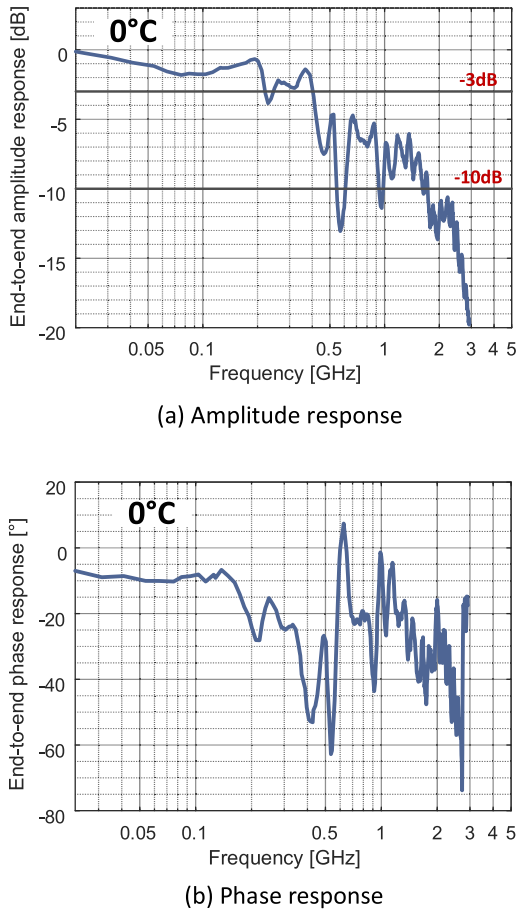

Fig. 8. The characterized (a) amplitude response and (b) phase response of the end-to-end system at 0 °C.

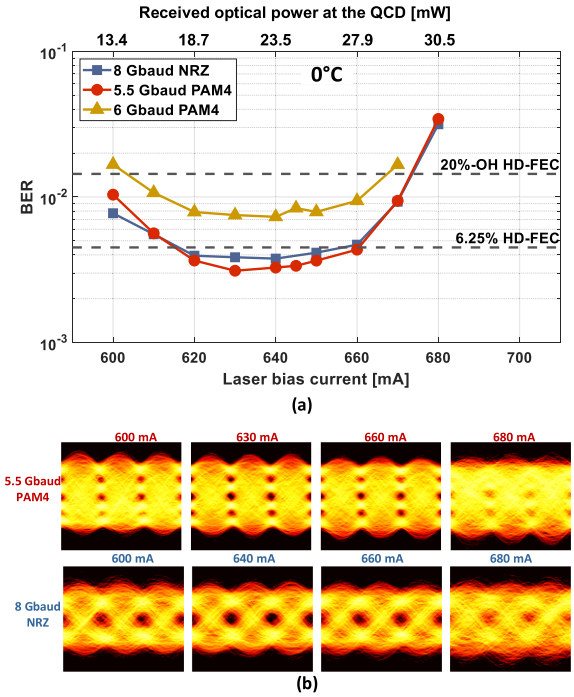

Fig. 9. (a) BER as a function of the laser bias current for NRZ-OOK signal at 8 Gbaud and PAM4 signal at 5.5 Gbaud (11 Gb/s) and 6 Gbaud (12 Gb/s); (b) Selected eye diagrams for both the 5.5 Gbaud PAM4 and the 8 Gbaud NRZ-OOK signals measured at different laser bias points.

TABLE I
SUMMARY OF ACHIEVED TRANSMISSION RESULTS

QCL Temperature	Achieved transmission results	Benchmarked FEC thresholds
10°C	6 Gbps NRZ	KP4-FEC
	7 Gbps NRZ	6.25%-OH HD-FEC
	8 Gbps PAM4	6.25%-OH HD-FEC
5°C	8 Gbps NRZ	20%-OH HD-FEC
	10 Gbps PAM4	6.25%-OH HD-FEC
0°C	8 Gbps NRZ	6.25%-OH HD-FEC
	11 Gbps PAM4	6.25%-OH HD-FEC
	12 Gbps PAM4	20%-OH HD-FEC

expected by further decreasing the QCL operation temperature below 0 °C to achieve higher QCL output power. However, it requires extra measures to prevent condensation on the QCL mount, which we will implement in our next-phase studies

IV. CONCLUSION

We demonstrated high-speed LWIR FSO transmissions at 9.6 μm wavelength with a directly-modulated QCL and a fully passive QCD without any cooling or bias voltage. The system supports up to 11 Gb/s bitrate with BER below the 6.25%-OH HD-FEC limit, verifying excellent bandwidth and linearity characteristics of both the DM-QCL and the QCD. This work is considered a significant milestone in the uncharted territory bitrate of >10 Gb/s LWIR FSO and shows the optimistic possibility of DM-QCL and QCD for the future ICT infrastructure and is a significant step towards a fully connected high-speed mid-IR FSO network, envisioned to be a promising alternative to the RF-based wireless systems.

REFERENCES

[1] Z. Zhang et al., "6G wireless networks: Vision, requirements, architecture, and key technologies," *IEEE Veh. Technol. Mag.*, vol. 14, no. 3, pp. 28–41, Sep. 2019.
[2] X. You et al., "Towards 6G wireless communication networks: Vision, enabling technologies, and new paradigm shifts," *Sci. China Inf. Sci.*, vol. 64, no. 1, pp. 1–74, 2020.
[3] X. Pang et al., "Bridging the terahertz gap: Photonics-assisted free-space communications from the submillimeter-wave to the mid-infrared," *J. Lightw. Technol.*, vol. 40, no. 10, pp. 3149–3162, May 2022.
[4] A. Delga and L. Leviandier, "Free-space optical communications with quantum cascade lasers," in *Proc. Quantum Sens. Nano Electron. Photon. XVI*, 2019, vol. 10926, Art. no. 1092617.
[5] J. J. Liu et al., "Mid and long-wave infrared free-space optical communication," in *Proc. Laser Commun. Propag. Atmos. Oceans VIII*2019, vol. 11133, Art. no. 1113302.
[6] A. K. Majumdar et al., *Free-space Laser Communications: Principles and Advances*, vol. 2. New York, NY, USA: Springer, 2010.
[7] E. Ip et al., "QPSK transmission over free-space link at 3.8 μm using coherent detection with wavelength conversion," in *Proc. 34th Eur. Conf. Opt. Commun.*, 2008, pp. 1–2.
[8] K.-D. F. Büchter, H. Herrmann, C. Langrock, M. M. Fejer, and W. Sohler, "All-optical Ti: PPLN wavelength conversion modules for free-space optical transmission links in the mid-infrared," *Opt. Lett.*, vol. 34, no. 4, pp. 470–472, 2009.
[9] Q. Hao et al., "Mid-infrared transmitter and receiver modules for free-space optical communication," *Appl. Opt.*, vol. 56, no. 8, pp. 2260–2264, 2017.
[10] Y. Su et al., "10 Gbps DPSK transmission over free-space link in the mid-infrared," *Opt. Exp.*, vol. 26, no. 26, pp. 34515–34528, 2018.
[11] W. Wang et al., "5 Gbaud QPSK coherent transmission in the mid-infrared," *Opt. Commun.*, vol. 466, 2020, Art. no. 125681.
[12] K. Zou et al., "Demonstration of free-space 300-Gbit/s QPSK communications using both wavelength- and mode-division-multiplexing in the mid-IR," in *Proc Opt. Fiber Commun. Conf. Exhibit.*, 2021, pp. 1–3.
[13] J. Faist, F. Capasso, D. L. Sivco, C. Sirtori, A. L. Hutchinson, and A. Y. Cho, "Quantum cascade laser," *Science*, vol. 264, no. 5158, pp. 553–556, 1994.
[14] M. Graf, N. Hoyler, M. Giovannini, J. Faist, and D. Hofstetter, "InP-based quantum cascade detectors in the mid-infrared," *Appl. Phys. Lett.*, vol. 88, no. 24, 2006, Art. no. 241118.
[15] Y. Bai et al., "Room temperature continuous wave operation of quantum cascade lasers with 12.5% wall plug efficiency," *Appl. Phys. Lett.*, vol. 93, no. 2, 2008, Art. no. 021103.
[16] M. Beck et al., "Continuous wave operation of a mid-infrared semiconductor laser at room temperature," *Science*, vol. 295, no. 5553, pp. 301–305, 2002.
[17] J. Faist et al., "Distributed feedback quantum cascade lasers," *Appl. Phys. Lett.*, vol. 70, no. 20, pp. 2670–2672, 1997.
[18] S. Bartalini et al., "Measuring frequency noise and intrinsic linewidth of a room-temperature DFB quantum cascade laser," *Opt. Exp.*, vol. 19, no. 19, pp. 17996–18003, 2011.
[19] N. Mustafa, L. Pesquera, C. Y. L. Cheung, and K. A. Shore, "Terahertz bandwidth prediction for amplitude modulation response of unipolar intersubband semiconductor lasers," *IEEE Photon. Technol. Lett.*, vol. 11, no. 5, pp. 527–529, May 1999.
[20] F. Capasso et al., "Quantum cascade lasers: Ultrahigh-speed operation, optical wireless communication, narrow linewidth, and far-infrared emission," *IEEE J. Quantum Electron.*, vol. 38, no. 6, pp. 511–532, Jun. 2002.
[21] M. Carras et al., "Room-temperature continuous-wave metal grating distributed feedback quantum cascade lasers," *Appl. Phys. Lett.*, vol. 96, no. 16, 2010, Art. no. 161105.
[22] X. Pang et al., "Gigabit free-space multi-level signal transmission with a mid-infrared quantum cascade laser operating at room temperature," *Opt. Lett.*, vol. 42, no. 18, pp. 3646–3649, Sep. 2017.
[23] X. Pang et al., "Free-space communications enabled by quantum cascade lasers," *Physica Status Solidi (a)*, vol. 218, no. 3, 2021, Art. no. 2000407.

[24] O. Spitz et al., "Free-space communication with directly modulated mid-infrared quantum cascade devices," *IEEE J. Sel. Topics Quantum Electron.*, vol. 28, no. 1, Jan./Feb. 2022, Art. no. 1200109.
[25] X. Pang et al., "Direct modulation and free-space transmissions of up to 6 Gbps multilevel signals with a 4.65-μm quantum cascade laser at room temperature," *J. Lightw. Technol.*, vol. 40, no. 8, pp. 2370–2377, Apr. 2022.
[26] A. Pavelchek et al., "Long-wave infrared (10- μm) free-space optical communication system," in *Proc. Free-Space Laser Commun. Act. Laser Illumination III*, pp. 247–252, vol. 5160, 2004.
[27] P. Martyniuk, W. Gawron, and J. Mikołajczyk, "The development of the room temperature LWIR HgCdTe detectors for free space optics communication systems," in *Proc. Adv. Free-Space Opt. Commun. Techn. Appl. III*, 2017, vol. 10437, Art. no. 104370G.
[28] O. Spitz, K. Yang, A. Guillaume-Manca, P. Didier, J. Liu, and F. Grillot, "Multi-Gb/s free-space communication with energy-efficient room-temperature quantum cascade laser emitting at 8.1 μm," in *Proc. IEEE Photon. Conf.*, 2021, pp. 1–2.
[29] H. Dely et al., "10 Gbit s^{-1} free space data transmission at 9 μm wavelength with unipolar quantum optoelectronics," *Laser Photon. Rev.*, vol. 16, no. 2, 2022, Art. no. 2100414.
[30] A. Bigioli et al., "Long-wavelength infrared photovoltaic heterodyne receivers using patch-antenna quantum cascade detectors," *Appl. Phys. Lett.*, vol. 116, no. 16, 2020, Art. no. 161101.
[31] X. Pang et al., "11 Gb/s LWIR FSO transmission at 9.6 μm using a directly-modulated quantum cascade laser and an uncooled quantum cascade detector," in *Proc. Opt. Fiber Commun. Conf. Exhib.*, 2022, pp. 1–3.
[32] L. M. Zhang and F. R. Kschischang, "Staircase codes with 6% to 33% overhead," *J. Lightw. Technol.*, vol. 32, no. 10, pp. 1999–2002, May 2014.
[33] P. Reininger et al., "Diagonal-transition quantum cascade detector," *Appl. Phys. Lett.*, vol. 105, no. 9, 2014, Art. no. 091108.
[34] T. Dougakiuchi et al., "Ultimate response time in mid-infrared high-speed low-noise quantum cascade detectors," *Appl. Phys. Lett.*, vol. 118, no. 4, 2021, Art. no. 041101.